THE JOURNAL OF PHYSICAL CHEMISTRY C
A JOURNAL OF THE AMERICAN CHEMICAL SOCIETY

pubs.acs.org/JPCC

Article

Paramagnetic Intrinsic Point Defects in Alkali Phosphate Glasses: Unraveling the P_3 Center Origin and Local Environment Effects

Luigi Giacomazzi,* Nikita S. Shcheblanov, Layla Martin-Samos, Mikhail E. Povarnitsyn, Shinji Kohara, Matjaž Valant, Nicolas Richard, and Nadège Ollier

Cite This: *J. Phys. Chem. C* 2021, 125, 8741−8751

Read Online

ACCESS | Metrics & More | Article Recommendations | Supporting Information

ABSTRACT: In this work, we carry out a first-principles investigation of intrinsic paramagnetic point defects in P_2O_5 and in $Na_2O-P_2O_5$ glasses as a representative of alkali phosphate glasses. Glass models are generated by combining classical molecular dynamics and Monte Carlo simulations and validated by comparing their corresponding structure factors with the available X-ray and neutron scattering experiments. We use density functional theory to calculate the electron paramagnetic resonance parameters for a large set of paramagnetic oxygen-vacancy configurations. Our investigation, also by unveiling the effect of the local environment and disorder on the hyperfine tensor, enables us to propose a new model for the much debated P_3 center. In particular, we establish the occurrence of two variants, which we name P_3^a and P_3^b centers, that are instrumental to explaining the experimental shifts of the hyperfine splittings observed in alkali phosphate glasses as a function of the alkali content x in the phosphate glass. Our scenario predicts that for low to intermediate alkali contents ($0 < x < 50\%$), a mixture of P_1 and P_3^a centers should be generated under irradiation. For $x > 50\%$, essentially only P_3^a and P_3^b centers would be generated, while P_1 will be absent. Therefore, our findings, by providing an improved mapping of P centers in phosphate glasses, pave the way for fine-controlling/tuning the optical absorption in a wide range of technological applications.

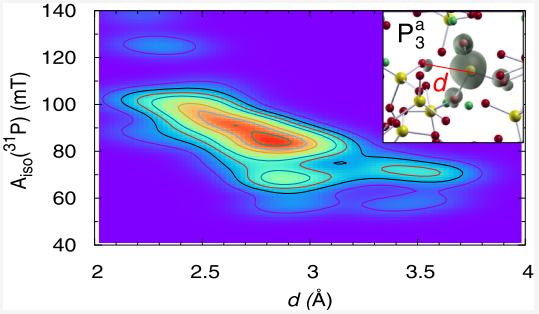

1. INTRODUCTION

Phosphate-based glasses have been the object of considerable interest during the last 3 decades because of their unique optical and physical properties.[1−8] For instance, phosphate-based glasses are biocompatible and thus can be employed to develop *in vivo* applications such as bioresorbable optical fibers.[9] Furthermore, as phosphate glasses exhibit a high solubility of laser-active rare-earth ions and a low thermo-optic coefficient, they are suitable materials for high-power lasers and fiber amplifiers.[2,10−12] Thanks to their low T_g, phosphate-based glasses are also currently foreseen as sealing materials for future laser welding applications.[13] In addition, phosphate glasses, and in particular Ag-doped phosphate glasses, have been widely employed for dosimetry applications.[14,15] Interestingly enough, several of the abovementioned applications rely on and can benefit from a proper understanding and controlling of point defects in phosphate glasses.

The detailed study of the network topology of sodium phosphate glasses started in the 1950s.[16−18] Since then, it became clear that the network topology in alkali phosphate glasses mainly consists of long chains of connected PO_4 units cross-linked, eventually, to other chains by metal cations through nonbridging oxygen atoms.[19] Depending on the number of nonbridging oxygen atoms at a given phosphate tetrahedron, the PO_4 unit is addressed as Q^3, Q^2, and Q^1 (or even Q^0) for one, two, and three nonbridging oxygen atoms, respectively. By incorporating alkali modifiers, such as Na_2O, into a P_2O_5 matrix, one can change the short- and intermediate-range order by inducing a further depolymerization of the network.[20−22] As a consequence, the concentration ratio Q^2/Q^3 increases with the alkali content (see also refs[22−24] for first-principles calculations). Consistently, the network of the $Na_2O-P_2O_5$ (or $NaPO_3$) glass, which is stoichiometric in the ratio between P and the alkali modifier Na_2O, is regarded as to be based on Q^2 units only,[25−27] at variance with the ideal network topology of pure P_2O_5 glass, which is based on Q^3 units only.[28]

Contrary to the broad agreement reached by the community on the main features of the network topology, experimental results and derived hypotheses on defect centers are scarce and sometimes controversial.[29,30] Investigation of point defects in irradiated phosphate glasses started in the 1960s on sodium metaphosphate ($NaPO_3$).[31,32] Weeks and Bray[33] found, by

Received: December 18, 2020
Revised: March 26, 2021
Published: April 16, 2021

https://doi.org/10.1021/acs.jpcc.0c11281
J. Phys. Chem. C 2021, 125, 8741−8751

means of electron paramagnetic resonance (EPR) spectroscopy, three signals, labeled P_1, P_2, and P_3, two of which were related to the formation of oxygen-deficient centers (P_1 and P_3). The hyperfine splittings (hfs) shown by the P_1, P_2, and P_3 signals are ∼95, ∼130, and ∼70 mT, respectively.[33] In more recent years, hfs similar to those of the P_1 or P_3 centers have also been found in fluoride phosphate[34−37] and in zinc phosphate glasses.[38]

While the identification of the point defects originating P_1 and P_2 centers is not under debate, the origin of the P_3 center has remained rather elusive. Weeks and Bray[33] refer to an electron trapped at a nonbridging oxygen vacancy as an explanation of EPR signals such as P_3. In ref 32, a 72.5 mT doublet (P_3) in the electron spin resonance (ESR) spectrum of sodium polyphosphate glass was attributed to the presence of a hole trapped by a three-fold coordinated phosphorus atom, that is, a PO_3 unit. More recently, Bocharova *et al.*[37] reaffirmed the association of doublets with hfs ∼70−80 mT to the occurrence of three-fold-coordinated phosphorus atoms, however, without being conclusive about the nature of their hole- or electron-trapped centers. Although it has recently been remarked by Pukhkaya *et al.*[29] that a Q^2 unit is required as a precursor for P_3 center formation and that P_3 is likely to be a hole trap, the electronic structure model of the P_3 center is still under debate, and hypotheses formulated so far (*e.g.*, a P_1 defect in a deformed PO_4 tetrahedron[29]) rely on little data, chiefly on hyperfine parameters.

Concerning the g tensor principal values, the available data are contradictory. For example, the data from Ebeling *et al.*[39,40] report of EPR centers in metaphosphate glasses, in particular of an electron-trapped paramagnetic center at threefold-coordinated P, regarded as responsible for a hyperfine doublet with hfs of ∼80−90 mT and with $g \simeq 2.064$. These data disagree with those of Weeks and Bray[33] who provide a value $\langle g \rangle \leq 2.02$ for P_1 and P_3 centers.[41]

In order to provide a clue to settle the long-standing debate, a modeling study from first principles is highly essential. However, in contrast to the case of point defects in crystalline materials, the study of point defects in glasses is significantly more complex. It is, first, necessary to generate reliable structural models, large enough to include solid-state effects. In addition, because of the structural disorder, the local environment of the point defect can vary sensibly from a site to another. Thus, the size of models should provide large enough statistics to take into account inhomogeneous broadening, which is essential to improve our understanding of physicochemical properties and/or to predict the behavior of defects.

In this work, we generate reliable glass models to discuss the structural origin and assignment of P centers in phosphates and metaphosphate glasses by means of density functional theory (DFT)-based EPR spectroscopy. The stochastic nature of the local environment in the glass has been taken into account not only through extensive first-principles calculations but also, as obtained therefrom, by means of suitable bivariate normal distribution broadenings which help to clarify the effect of spatial variations on EPR parameters. Such a representation provides an improved picture of how the local environment impacts on EPR parameters and allows for more straightforward and meaningful comparisons with the experimental results. In particular, by considering the oxygen vacancies generated in $NaPO_3$, P_2O_5, and P-doped SiO_2 glass models and, on the basis of systematic cross-checks and comparisons, allowing to overcome possible DFT biases and scarcity of experimental data, we propose a new model for explaining the origin of the debated P_3 center. Essentially, we establish the occurrence of two variants, which we name P_3^a and P_3^b centers. The calculated relative Fermi contact of P_3^a with respect to P_1 is in agreement with the experimental differences of hfs available for P_1 and P_3 centers. Finally, the proposed existence of two variants of the P_3 centers allows explaining the observed shifts of the Fermi contacts for varying alkali contents.

2. METHODS

The calculations presented in this work are based on DFT. The codes we used are freely available with the Quantum-Espresso package.[42,43] The Perdew−Burke−Ernzerhof (PBE) exchange correlation functional[44] has been adopted for the present calculations due to its reliability proven in similar systems.[45,46] Norm-conserving Trouiller−Martins pseudopotentials are used,[47] and Kohn−Sham wave functions are expanded on the basis of plane waves up to a kinetic cutoff of 70 Ry.

The point-defect configurations analyzed hereafter have been obtained using two models of sodium phosphate (SP) glass (*i.e.*, $NaPO_3$) consisting of a periodic supercell containing 100 atoms (480 valence electrons) with 20 regular corner-sharing PO_4 tetrahedral units. Regular PO_4 units in P_2O_5 and in $(Na_2O)_x$−$(P_2O_5)_{1-x}$ glasses may exhibit one, two, or three normal P−O bonds, where O is a bridging oxygen atom, and correspondingly three, two, and one P−O_{nb} bonds, where O_{nb} is a nonbridging oxygen atom (P−O_{nb} bond might be P−O or P═O, where "═" refers to a double bond or π-bonding according to some authors[21]). Such PO_4 units are hereafter referred to as Q^1, Q^2, and Q^3 tetrahedral units, respectively. By means of the reverse Monte Carlo (RMC) approach, we generate a model with 100 atoms, hereafter labeled the RMC-SP model. RMC modeling is performed using the RMC++ code.[48−50] For the RMC model generation, in the first step, we perform an initial hard-sphere Monte Carlo run (*i.e.*, RMC w/o diffraction data) with the following constraints: each P atom is coordinated by two nonbridging oxygen atoms at a distance of 1.4−1.5 Å and two bridging oxygen atoms at 1.5−1.7 Å; each nonbridging oxygen atom is coordinated by one P atom at a distance of 1.4−1.5 Å, while each bridging oxygen atom is coordinated by two P atoms at a distance of 1.5−1.7 Å. In the second step, we run RMC with X-ray and neutron structure factors, $S(Q)$.[51]

The numerical procedure adopted for the generation of a $NaPO_3$ glass model using classical molecular dynamics (hereafter labeled CMD-SP) is based on ref 52. The CMD simulations are carried out with the help of the LAMMPS code.[53] The atomic coordinates of atoms, as obtained by RMC and CMD modeling, were refined further by means of a first-principles relaxation (force threshold, 0.0025 eV/Å). Geometry optimizations of the undefected models and of oxygen-vacancy configurations have been carried out through spin-polarized calculations. Configurations of paramagnetic centers are obtained by removing a terminal oxygen from one PO_4 tetrahedron and then by performing a first-principles relaxation of the atomic structure which is put in a positive charge state. Next, EPR parameters (the hyperfine tensors $\mathbf{A}$ and g tensors[54]) are calculated using the QE-GIPAW code. The latter code exploits the gauge including projector augmented wave (GIPAW) method for the calculation of the EPR parameters.[55] EPR g tensor calculations were performed using a convergence threshold of 5×10^{-14} Ry^2 for the

https://doi.org/10.1021/acs.jpcc.0c11281
J. Phys. Chem. C 2021, 125, 8741−8751

diagonalization and for Green's function solver of the QE-GIPAW module. We also investigate the oxygen-vacancy paramagnetic centers in two recently generated models[28] of vitreous P_2O_5, both consisting of a 112-atom supercell with 32 regular corner-sharing PO_4 tetrahedral units. Moreover, for dedicated comparisons, configurations of the P_1 center in silica (*i.e.*, P-doped silica) have been obtained by replacing the three-fold Si in the representative configurations of the E'−Si center[56] with a three-fold *P*, where the cell is doubly charged, so as to generate a *P* point defect isoelectronic with the E'−Si center.[59]

We note that for paramagnetic centers such as the P_1 center, featuring an sp^3 spin density spread over a few atoms, the calculation of Fermi contacts at the DFT level is well justified in extended systems,[56] and the use of hybrid functionals is not crucial. In fact, as shown by Pacchioni *et al.*,[57] using cluster models, for the P_1 center in P-doped SiO_2, the Fermi contact $A_{iso}(^{31}P)$ calculated at DFT (B3LYP) levels differs by ∼5% with respect to experiments.[58] With the present DFT setup for the configurations of the P_1 center in P-doped SiO_2, we calculate $A_{iso}(^{31}P)$ differing from experiments at most by ∼10% (Table 2). Furthermore, we carried out a few test calculations of $A_{iso}(^{31}P)$ for the representative configurations of the P_1, P_3^a, and P_3^b centers using a PBE0 hybrid functional to calculate the spin density at the relaxed PBE geometry. Usage of PBE0 has led to similar increments of ∼7% for all the tested configurations with respect to PBE (Supporting Information Table S1). However, such a variation does not affect the conclusions of the present work which are based on relative differences.

3. RESULTS

3.1. Sodium Phosphate Glass Models: Structural Details. For assessing the quality of our model structures, we present the neutron and X-ray structure factors in Figure 1. We find an overall reasonable agreement with the experimental data.[51] The calculated $S(q)$ in the short-range order ($q \geq 4$ Å^{-1}), which reflects the basic tetrahedral PO_4 unit, agrees well with the experimental data. Moreover, both our models RMC-SP and CMD-SP feature first diffraction peaks at about 1.6−2.0 Å^{-1} in the neutron $S(q)$, indicating a fair enough description of the intermediate-range order (periodicity up to ∼4 Å[20]), which mainly reflects the arrangement of atoms in neighboring phosphate chains. The agreement achieved in Figure 1 allows us to infer that our models of sodium phosphate glasses satisfactorily describe the surrounding environment of the point defects presented hereafter.

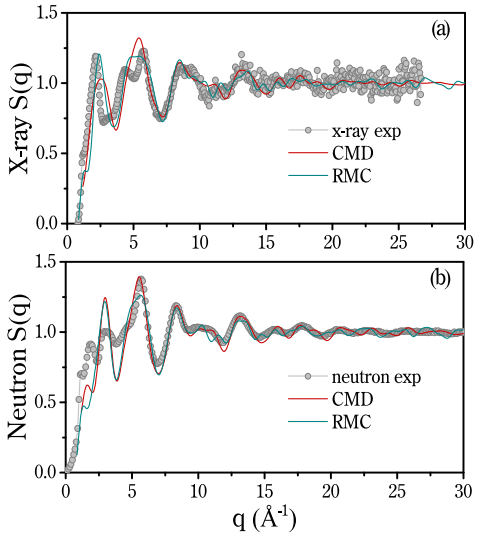

Figure 1. (a) X-ray and (b) neutron structure factor $S(Q)$, as found in experiments (discs)[51] and as calculated for the models CMD-SP (red solid line) and RMC-SP (green solid line) of $NaPO_3$ glass.

In Table 1 we provide a list of the structural models of sodium phosphate ($NaPO_3$) and P_2O_5 glasses that we have employed for the present study, together with their Q^n speciation. The models RMC1−P_2O_5 and RMC-SP feature Q^3 and Q^2 units only, while RMC2−P_2O_5 also shows a minor fraction of Q^2 and Q^4 units besides Q^3 units. The model CMD-SP is mainly based on Q^2 units, although it shows a noticeable fraction of Q^1 and Q^3 units and one single penta-coordinated P atom (Q^5 unit).

Table 1. Q^n Speciation (in %) of Models of P_2O_5 and Sodium Phosphate ($NaPO_3$) Glasses

P_2O_5	*N*	Q^1	Q^2	Q^3	Q^4	Q^5
RMC1−P_2O_5	112			100		
RMC2−P_2O_5	112		3	87	10	
$NaPO_3$	*N*	Q^1	Q^2	Q^3	Q^4	Q^5
CMD−SP	100	15	70	10		5
RMC−SP	100		100			

[a] *N* is the number of atoms in the simulation cell. For P_2O_5 models, the data are taken from ref 28.

At variance with the RMC-SP model made of 100% Q^2 units, as expected for the $NaPO_3$ glass,[26,27] we note that models obtained by means of classical molecular dynamics are not so realistic as they contain sizeable fractions of Q^1 and Q^3 units.[52,60] In fact, the appearance of Q^1 and Q^3 is intrinsically related to the CMD atomistic description based on simple interaction potentials.[52,60] Moreover, the presence of Q^5 units is also likely to be an artifact of classical molecular dynamics.[61,62] Although we are not aware of any experimental data about Q^5 units in alkali phosphate glasses, we remark that Q^5 units might appear in melt phases.[63] However, from a macroscopic dielectric point of view, the presence of a few Q^1, Q^3, and Q^5 units in CMD-SP does not substantially alter its dielectric response. We have calculated at the DFT level, using the linear response code ph.x of the QE,[42,45] a high-frequency dielectric constant of 2.35 for the CMD-SP model and of 2.33 for the RMC-SP model, with only 1% difference. Hence, both models will provide an equivalent screening when a charged point defect is present and can be used for the purposes of the present paper, that is, to consider $NaPO_3$ glass models which, by means of the distribution of Q^n units, allow for investigations also relevant for a wide range of $xNa_2O-P_2O_5$ glasses.

The $NaPO_3$ glass is thought to consist of Q^2 units only.[27] By contrast, in $(Na_2O)_x-(P_2O_5)_{1-x}$ glasses, Q^1 and Q^3 units are also present.[22,27] Thus, the sodium phosphate models we have generated in this work, by presenting a variety of speciation Q^n (Table 1), not only allow for the investigation of point defects in $NaPO_3$ glass which consists of Q^2 units only but are also meaningful for wider classes of phosphate glasses.

3.2. EPR Centers in P_2O_5 Glass. In this section, we discuss the oxygen-vacancy-related EPR centers in P_2O_5 using the models generated in ref 28. The results obtained are not only

https://doi.org/10.1021/acs.jpcc.0c11281
J. Phys. Chem. C 2021, 125, 8741−8751

Table 2. Fermi Contacts A_{iso} (^{31}P) (mT) and Anisotropic Parameters B_j (mT) of P_1 and P_2 Centers in P_2O_5 Glass (RMC1−P_2O_5 Model) as Calculated by First-Principles in This Work (T.W.), Together with Their SDs (in Parentheses),[a] and as Obtained in Experiments[33,58]

		glass	$A_{iso}(^{31}P)$	B_1	B_2	B_3
P_1	T.W.	P_2O_5	108.7(6.3)	−5.3(2)	−5.5(1)	10.8(3)
	T.W.	P-doped SiO_2	93.2(6.5)	−5.9(1)	−6.0(1)	12.0(2)
	expt.[33]	P_2O_5	95(12)			
	expt.[58]	P-doped SiO_2	91	−6.0	−6.0	12.0
P_2	T.W.	P_2O_5	142.7(7.8)	−4.8(3)	−5.4(2)	10.2(4)
	expt.[33]	P_2O_5	143.6(10)			
	expt.[58,66]	P-doped SiO_2	120	−4.4	−5.5	9.9

[a]In ref 33, hfs were measured as the separation between the points of maximum slope on the derivative curves, with the width (in parenthesis) given by the separation between the extremal inflection points of the derivative curve.

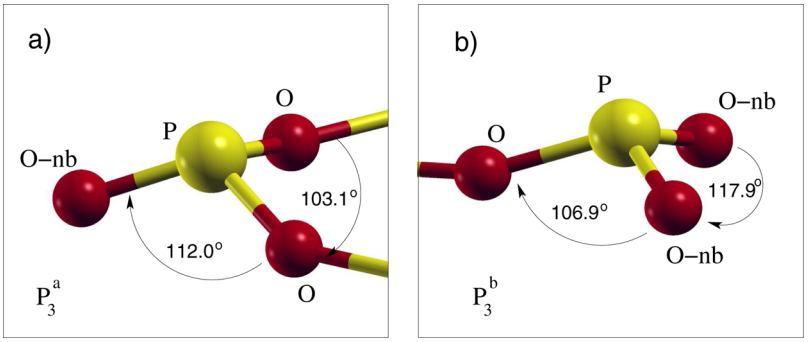

Figure 2. Sketch of P_3^a and P_3^b configurations (based on CMD-SP data) in $NaPO_3$ glass. For clarity, Na ions have been omitted. O−nb refers to nonbridging oxygen atoms.

interesting for the investigation of paramagnetic defects in P_2O_5 but also constitute a helpful benchmark for the EPR centers in sodium phosphate glasses, which is exploited in the next section. By following the procedure outlined in Section 2, we could generate P_1, P_2, and phosphorus−oxygen−hole-center (POHC) configurations in our models. As POHC centers are not relevant for the scope of the present study, their discussion is not included in this paper (the reader may consult ref 45.), and in the following, data are provided only for configurations classifiable as P_1 and P_2 centers. The P_1 and P_2 centers in P_2O_5-based glasses are structurally analogous to P_1 and P_2 centers in P-doped SiO_2,[58] with $A_{iso}(^{31}P)$ ∼85−95 and ∼120−140 mT, respectively.[33,39,64−66]

In the model RMC1−P_2O_5, by removing the nonbridging oxygen from Q^3 units, we could generate 16% configurations classifiable as P_1 centers. The other kinds of point defects obtained by first-principles relaxation are POHC (50%), P_2 (25%), and "P_2-like" (9%) configurations. The latter kind of configuration consists of a P_1 center which attracts a nonbridging oxygen atom (from the neighboring phosphate Q^3 units) and thus becomes almost coordinated to P_1 (with a P−O distance ∼ 2.2−2.4 Å). Consequently, the spin density of the "P_2-like" configuration resembles the one of a P_2 center, with a pseudo-trigonal-bipyramidal structure around the P atom[57,58] and a large $A_{iso}(^{31}P)$ ∼135 mT. Yet, following the cutoff distance criterion, these P_2-like configurations could still be classified as P_1 centers.

In Table 2, we report the Fermi contacts as calculated for P_1 and P_2 configurations generated in our RMC1−P_2O_5 model of P_2O_5 glass, together with the experimental data from refs 33 and 58. In irradiated pure P_2O_5, one can find P_1 and P_2 centers, which experimentally exhibit ∼95 and ∼143 mT hfs, respectively.[33] In the present calculations, we have found on average $A_{iso}(^{31}P)$ ∼108 and ∼141 mT for P_1 and P_2 configurations, respectively. We note that, for the P_1 center, the Fermi contact in P_2O_5 is slightly larger than that found in P-doped silica, both in theory and experiments.[33,58,66]

The average of $A_{iso}(^{31}P)$, as calculated for P_1 configurations in P_2O_5, overestimates the experimental estimate of ref 33 by ∼14 mT. In P-doped silica also, we found an overestimation of a few mT for the Fermi contact in P_1 configurations with respect to the experimental estimate of ref 58. For P_2 configurations in P_2O_5, the calculated (average) A_{iso} is in rather good agreement with the experimental data. As for P_2 configurations, the unpaired electron is in a 3s + 3p orbital on P,[57] whereas sp^3 orbital hosts the unpaired electron in the P_1 configuration, the larger discrepancy with respect to experiments registered for P_1 could be related to the different *s* weight in the sp hybridization. Concerning the anisotropic hyperfine interaction in P_1 centers (Table 2), our calculations support a slightly smaller value (5.4 mT) in P_2O_5 with respect to P-doped silica (∼6.0 mT), which is in good agreement with experiments.[33,58]

As far as the oxygen vacancies in the RMC2−P_2O_5 model are concerned, we focused on a specific case of interest. In particular, by removing the nonbridging oxygen atoms from Q^2 units (Table 1) in the model RMC2−P_2O_5, we obtained two paramagnetic point defects with a spin density similar to that of P_1 but where the three-fold coordinated *P* has one nearest-neighbor oxygen, which is a nonbridging oxygen atom (*i.e.*, a "P_3^a" configuration; see also Section 3.3 and Figure 2a). In such P_3^a configurations, $A_{iso}(^{31}P)$ ≃87.4 and ≃82.1 mT, respectively, that is, with an average underestimation of ∼24 mT in comparison with the calculated Fermi contact of P_1 configurations given in Table 2 (a snapshot of the spin

https://doi.org/10.1021/acs.jpcc.0c11281
J. Phys. Chem. C 2021, 125, 8741−8751

densities of P_1 and P_3^a configurations in P_2O_5 glass is provided in Supporting Information Figure S1).

The results shown in Table 3 for the g tensor of P_1 configurations indicate that in P_2O_5, the g principal values are larger than that in P-doped silica. Both theory and experiments support an increase in the g values of up to ≃5000 ppm in P_2O_5 with respect to P-doped silica. Moreover, the calculated g principal values support for the P_1 center an orthorhombic g tensor in both P_2O_5 and P-doped SiO_2. Also, in light of Table 3, the g tensor principal values of P_1 centers larger than 2.005 in P_2O_5-based glasses are unlikely.

Table 3. g Tensors of P_1 Centers in P_2O_5 and in P-Doped SiO_2 Glasses[67] as Calculated in This Work (T.W.), Together with Their SDs (in Parentheses), and as Obtained from Experiments (refs 33 and[58])

expt.		⟨g⟩	ref
P_2O_5		2.005	33
P-doped SiO_2	$g_\parallel$ = 2.002	$g_\perp$ = 1.999	58
theory (T.W.)	$g_1 = g_\parallel$	g_2	g_3
RMC1−P_2O_5	2.0041(7)	2.0026(7)	2.0017(3)
P-doped SiO_2	2.0022(1)	2.0015(3)	2.0010(3)

3.3. EPR Centers in Sodium Phosphate Glasses. In this section, we present the results of the calculations of the hyperfine couplings $A_{iso}(^{31}P)$ and g tensors for the charged oxygen vacancies generated in our models of $NaPO_3$ glass. The vast majority of Q^n units in our models belongs to the Q^2 type (see Table 1). From the removal of a nonbridging oxygen atom in Q^2 units, with a subsequent first-principles relaxation in the positively charged state, we could analyze about 80 paramagnetic configurations, the majority of which (71%) exhibits a structure as shown in Figure 2a: the threefold coordinated P atom is bonded to two bridging oxygen and one nonbridging oxygen atoms. Such a paramagnetic P center configuration is hereafter labeled as "P_3^a". On average, the P−O bonds have a length of 1.63 Å, with a standard deviation (SD) of 0.03 Å, whereas the P−O_{nb} bonds have a length of 1.50 Å with a SD of 0.01 Å. The O−P−O angle is on average 103.1° with a SD of 3.7°, whereas O−P−O_{nb} angles are 112° with a SD of 3.6°.

Besides the Q^2 units, the CMD-SP model also has three Q^1 units, corresponding to 15% of P atoms (Table 1), which allows for the generation of nine configurations of positively charged oxygen vacancies, as generated by removing a nonbridging oxygen atom and cycling over the total nine motifs. The structure of these centers (hereafter labeled as "P_3^b") consists of a three-fold-coordinated P atom bonded to one bridging oxygen and two nonbridging oxygen atoms, as shown in Figure 2b. The P−O bond with the oxygen-bridging atom is, on average, 1.68 Å long with a SD of 0.02 Å. The shorter P−O_{nb} bonds with the nonbridging oxygen atoms are on average 1.52 Å long, with a SD of 0.01 Å. The O_{nb}−P−O_{nb} angle is on average 117.9° with a SD of 4.6°, whereas the O−P−O_{nb} angles are about 106.9° with a SD of 2.9°.

Concerning the location of Na ions around the terminal oxygen atoms, in both P_3^a and P_3^b configurations, we have found three Na ions located at a distance of ≃2.5 Å from the nonbridging oxygen atoms, consistent with the Na−O lengths reported in the literature.[51,60]

Besides the ideal case shown in Figure 2a, we have also generated configurations (Figure 4a), at the Q^2 unit of the nonbridging oxygen vacancy site, where P becomes four-fold-coordinated or almost four-fold-coordinated.[68] In the latter configurations, the unpaired spin is hosted at a kind of [$(O-)_3P{=}O$] tetrahedron with a wide O−P−O or O−P═O angle of ∼150°. Such extremely "strained" P_3^a configurations typically show large $A_{iso}(^{31}P)$ values of about 100 mT. From the first-principles relaxation of a positively charged nonbridging oxygen vacancy at a Q^2 tetrahedron, we almost never obtained a P_3^b configuration. In fact, considering both our models CMD-SP and RMC-SP, only one P_3^b configuration was found, suggesting that Q^2 units give rise almost exclusively to the P_3^a kind of paramagnetic center. Our model CMD-SP also features two Q^3 units, which, after the removal of the nonbridging oxygen and subsequent relaxation in the positively charged state, provided a POHC configuration and a P_2 configuration with $A_{iso}(^{31}P)$ ≃117 mT.

In irradiated sodium phosphate glasses, the hfs assigned to the P_3 center correspond to $A_{iso}(^{31}P)$ ∼65−75 mT (Table 4), that is, 20−25 mT less than those found for P_1 centers.[29,33,58] The calculations carried out in this work show that the oxygen vacancies created at the Q^1 and Q^2 units lead to a $A_{iso}(^{31}P)$ distribution (Figure 3) rather wide (∼50−120 mT), which covers the experimental range of hfs reported for the P_3 center. In our models CMD-SP and RMC-SP (Table 1), the average values of the Fermi contact of P_3^a configurations generated at Q^2 units are 85.4 and 85.2 mT, respectively. The latter averages are compatible with the peaks at ∼75 and ∼85 mT of the distributions displaced in Figure 3, consistent with the fact that P_3^a represents the majority of nonbridging oxygen-vacancy configurations obtained at the Q^2 units. Overall, the Fermi contact of the analyzed P_3^a configurations shows an average around ∼85.3 mT, which is ∼20−25 mT less than that calculated for P_1 in a pure P_2O_5 glass (Table 2). The average $A_{iso}(^{31}P)$ Fermi contact of the P_3^b configurations is 68.3 mT with a SD of 9.1 mT. Thus, we find a difference in $A_{iso}(^{31}P)$ of about 16 mT between the P_3^a and P_3^b configurations, consistent with the order of magnitude of the observed variation of the

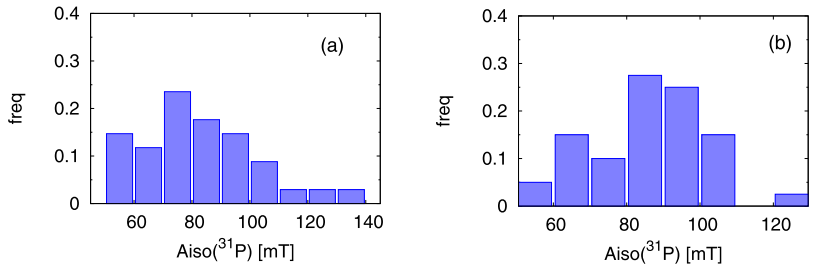

Figure 3. Distributions of $A_{iso}(^{31}P)$ (mT) of positively charged nonbridging oxygen vacancy configurations at Q^1 and Q^2 units, as calculated in our $NaPO_3$ glass models: (a) CMD-SP and (b) RMC-SP.

https://doi.org/10.1021/acs.jpcc.0c11281
J. Phys. Chem. C 2021, 125, 8741−8751

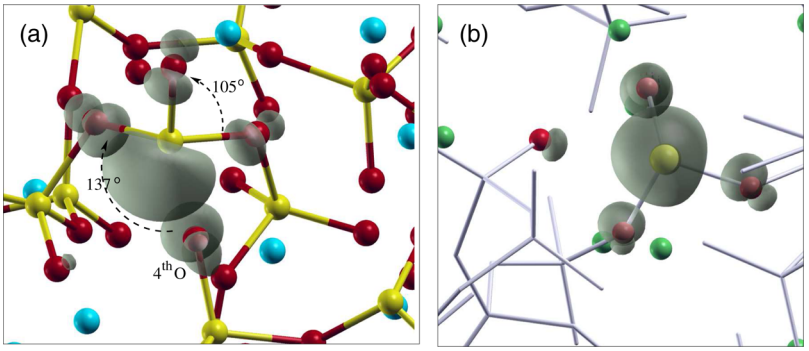

Figure 4. Spin density (shaded/gray), as calculated (a) for a P_3^a configuration (in model CMD-SP), which features a fourth next-nearest-neighbor oxygen atom at a distance of $d \simeq 2.2$ Å, showing the spin density localization and overall appearance as those of a P_2 center[58] and (b) for a typical case with $d > 2.2$ Å. The phosphate network is represented by a ball-and-stick model: bonds (sticks), P (yellow balls), O (red balls), and Na atoms (green balls) are shown. For clarity, in (b), only P and O atoms of the paramagnetic defect are shown.

Table 4. Fermi Contacts $A_{iso}(^{31}P)$ (mT) and Anisotropic (Dipolar) Hyperfine Values B_j in xNa$_2$O:P$_2$O$_5$ Glass as Calculated in This Work (T.W.), Together with Their SDs (in Parentheses),[a] and as Found in Experiments[33]

	X	$A_{iso}(^{31}P)$	width	B_1	B_2	B_3
			Expt.			
P_3	0.5	74.2	9.0			
P_3	0.57	66.5	9.0			
			Theory (T.W.)			
P_3^a	0.5	85.3(16.5)		−5.3(3)	−5.6(3)	10.8(5)
P_3^b	0.5	68.3(9.1)		−5.0(3)	−5.3(3)	10.3(6)

[a] x indicates the Na$_2$O content.

Fermi contacts in P_3 centers, varying from ∼66 to 74 mT in sodium phosphate glasses.[29,33]

In Figure 5a we show the Fermi contact $A_{iso}(^{31}P)$ of P_3^a configurations plotted *versus* the distance d between the threefold coordinated P and a fourth nearest-neighbor O atom featuring spin density localization (Figures 4 and 5b). Although for a given distance, the $A_{iso}(^{31}P)$ Fermi contacts exhibit large variations (*e.g.*, ∼30 mT at $d \sim 3$ Å), a trend is discernable so that the Fermi contact tends to decrease with the increasing distance d, for d between 2.2 and ∼3.5 Å. (In Supporting Information Figure S2, we show that, alternatively, one may consider the trend between Fermi contacts $A_{iso}(^{31}P)$ and the mean bond angle O−P−O, which reflects the degree of planarity of the PO_3 pyramid). From the distribution of Figure 5a, one can infer that configurations (Figure 4a) reminiscent of the P_2 center,[58] although with a distance $d \sim 2.5$ Å, well beyond the conventional P−O bond cutoff distance of 2.2. Å, can possess a large $A_{iso}(^{31}P)$ ∼90−100 mT. In Figure 5b, we provide the distribution of Fermi contacts $A_{iso}(^{17}O)$ on the fourth neighboring oxygen atom, as calculated for the P_3^a configurations in our sodium phosphate models. For small $d \sim 2.2$ Å, $A_{iso}(^{17}O)$ can exhibit values between −3 and −5 mT, close to those reported for axial oxygen atoms (−5 to −6 mT) in P_2 configurations.[57] By contrast, for d larger than ∼2.7 Å, the absolute value of the Fermi contact $A_{iso}(^{17}O)$ takes small values (≤1.5 mT), decreasing further with d, so that in this range of d the P_3^a center can be regarded as an ideal three-fold-coordinated P center. By means of a bivariate normal distribution and using suitable broadenings (0.2 Å and 5 mT), we obtain from the data points of Figure 5a a smooth distribution (Figure 5c) of A_{iso} *versus* d, which allows for an immediate reading of the information concerning the most likely $A_{iso}(^{31}P)$ and d values (i.e., 85 mT and $d \sim 2.8$ Å), the spreading (at $d \sim 2.8$ Å, the fwhm is ∼20 mT) and the trend, which is evident from the ridge of the distribution.

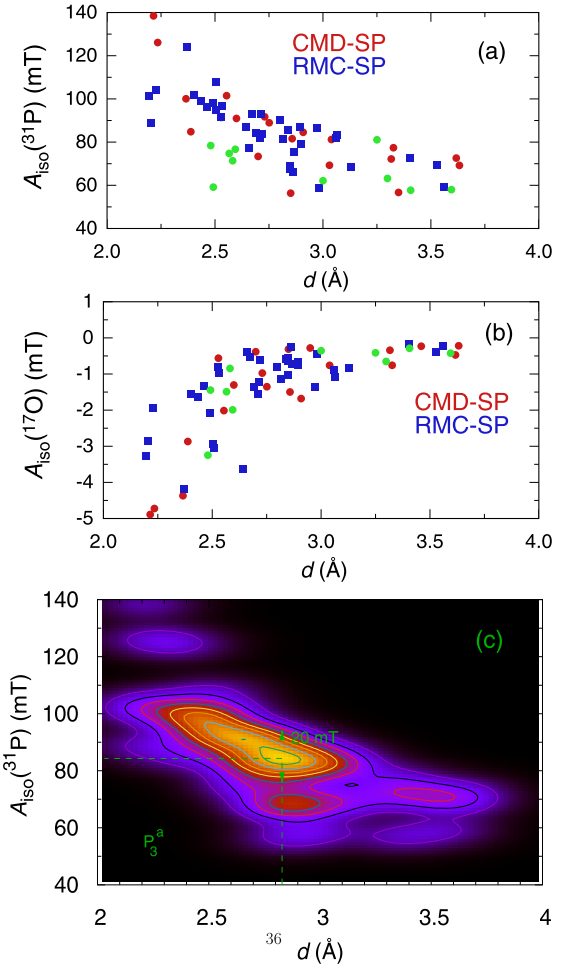

Figure 5. (a) Calculated Fermi contact $A_{iso}(^{31}P)$ of P_3^a configurations shows a trend *vs* the distance d between the three-fold-coordinated P and the fourth nearest-neighbor O atom featuring spin density localization. (b) Distribution of the Fermi contact $A_{iso}(^{17}O)$ of the fourth nearest-neighbor O *vs* d. (c) Smoothed distribution of the Fermi contact in P_3^a configurations obtained by the Gaussian broadening (0.2 Å and 5 mT) of the points shown in panel (a). The Fermi contacts of P_3^a configurations are also shown in panel (a,b) with light green discs.

https://doi.org/10.1021/acs.jpcc.0c11281
J. Phys. Chem. C 2021, 125, 8741−8751

Note that d represents the spatial extension of the unpaired electron wave function, which is sensitive to the local environment. In fact, we note that besides the Fermi contact, other hyperfine parameters also, for example, the anisotropic parameter B_3,[54] display a distribution, as shown in Figure 6a,

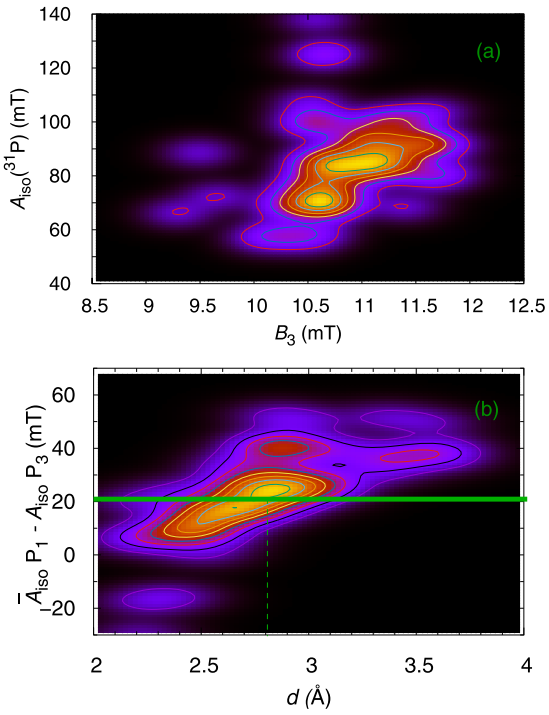

Figure 6. (a) Distribution of $A_{iso}(^{31}P)$ *vs* B_3 values for P_3^a configurations, that is, the distribution of sp hybridization in P_3^a configurations (Gaussian broadenings of 0.3 and 5 mT were applied for B_3 and A_{iso}, respectively). (b) Relative difference between $\bar{A}_{iso}(^{31}P)$ in P_1 and $A_{iso}(^{31}P)$ in P_3 configurations. Experimental shift between P_1 and P_3 is shown as a solid green line (expt. data taken from ref 33).

which reflects the distribution given in Figure 5. As the $A_{iso}(^{31}P)$ and B_j parameters are related to the weight of the s and p components of the unpaired wave function,[33] the distribution in Figure 6a basically describes the variation of the sp hybridization among our P_3^a configurations which in turn depends on the local environment, for example, d parameter (See also Supporting Information Figure S2), and thus is also reflected in other distributions as, for example, Figure 5. In Figure 6b, we provide the relative difference between the average Fermi contact $A_{iso}(^{31}P)$ of P_1 configurations in P_2O_5 and Fermi contacts of P_3^a configurations. Such a distribution shows a peak at ∼23 mT for a distance d ∼ 2.8 Å, which is immediately seen to be consistent with the relative difference (21 mT) of hfs in P_1 and P_3 centers.[33]

As far as P_3^b configurations are concerned, given the small number of configurations, we are not able to argue about the existence of the dependence of $A_{iso}(^{31}P)$ on d (Figure 5a), although the Fermi contact $A_{iso}(^{17}O)$ on the fourth neighboring oxygen atom in P_3^a configurations seems to follow the same distribution as in P_3^a configurations (Figure 5b). Yet, the group of P_3^b configurations at d ∼ 2.5 Å shows $A_{iso}(^{31}P)$ in the range 60−80 mT and hence may not follow the trend displayed by P_3^a configurations.

The g tensor principal values in P_3^a configurations display only a weak dependence on the distance d from the fourth nearest-neighbor oxygen atom (not shown), so that we hereafter just provide the average g tensor data. The averages of g tensor values as calculated for P_3^a configurations of the CMD-SP and RMC-SP models are the following: g_1 = 2.0042(6), g_2 = 2.0030(4), and g_3 = 2.0011(6), which are rather close to the g tensor principal values ($g_\parallel$ = 2.0041, $g_\perp$ = 2.0026 and 2.0017) calculated for P_1 configurations in vitreous P_2O_5 (Table 3). As far as the P_3^b configurations are concerned, we found g tensor principal values of g_1 = 2.0043(6), g_2 = 2.0026(3), and g_3 = 2.0005(9), slightly more orthorhombic than in P_3^a and P_1 (Table 5). Although a deviation of ∼1000 ppm could occur between the calculated and real $\langle g \rangle$ of the P_3 center,[69] the present data, thus, support a lower $\langle g \rangle$ with respect to the value of ∼2.01 given by ref 33. The fact that the calculated spin density of a P_3^a configuration, Figure 4b, is similar to the one of the P_1 center also provides support for a paramagnetic center model with EPR parameters reasonably close to those observed for the P_1 center and thus further casting some doubts about $\langle g \rangle \simeq 2.01$ given by ref 33.

Table 5. g Tensors in P_2O_5 and $NaPO_3$ Glasses for P_1, P_3^a, and P_3^b Configurations, as Calculated in This Work (T.W.), with Their SDs (in Parentheses), Compared to Experimental Data Available for P_1 and P_3 Centers[33]

experiment[33]				
center		glass		$\langle g \rangle$
P_1		P_2O_5		2.005
P_3		$NaPO_3$		2.012
theory (T.W.)				
center	Glass	g_1	$g_2 = g_\parallel$	g_3
P_1	P_2O_5	2.0026(7)	2.0041(7)	2.0017(3)
P_3^a	$NaPO_3$	2.0042(7)	2.0030(4)	2.0011(7)
P_3^b	$NaPO_3$	2.0043(6)	2.0026(3)	2.0005(9)

4. DISCUSSION

The assignments done in the present work are mainly based on the relative comparison between P_1 and P_3 configurations in P_2O_5 and in $NaPO_3$ glasses. For a given system and for a properly chosen EPR parameter, for example, $A_{iso}(^{31}P)$, comparing the relative differences between the different centers provides a reliable way to make assignments substantially not affected by method-dependent errors.[56,70] The P_3^a configurations in our $NaPO_3$ glass models present an average $A_{iso}(^{31}P)$ of ∼85 mT, about 24 mT less than the calculated average A_{iso} of P_1 configurations in P_2O_5 (Table 2). For comparison, Weeks and Bray[33] report a value of 95 mT for the experimental hfs of the P_1 center in P_2O_5 glass and 74 mT for the hfs of the P_3 center in $Na_2O-P_2O_5$ glass, that is, a 21 mT difference (Figure 6b).

On the basis of the Fermi contact distributions shown in Figures 5 and 6, we infer that the P_3 center is, above all, a nonbridging oxygen vacancy generated at a Q^2 unit, for which an example of spin density is provided in Figure 4 or, to a lesser extent, to a Q^1 unit. There is a considerable difference (∼16 mT) between the calculated Fermi contacts of paramagnetic oxygen vacancy configurations generated at Q^1 and at Q^2 units, that is, the centers P_3^b and P_3^a, respectively. Such a difference may be helpful to explain the range of values given by the available experimental data in alkali phosphate glasses featuring different ratios of Q^2 to Q^1 units (in Weeks and Bray:[33] 66−78 mT).

https://doi.org/10.1021/acs.jpcc.0c11281
J. Phys. Chem. C 2021, 125, 8741−8751

Only one P_3^b, but neither P_1 nor P_2, configuration has been obtained by the first-principles relaxations of the positively charged oxygen vacancies at Q^2 units in our $NaPO_3$ glass models. Hence, the calculations carried out on the CMD-SP and RMC-SP models suggest that the ionization of a nonbridging oxygen vacancy at a Q^2 unit may give rise to only P_3^a configurations.

From the present findings, in particular, the fact that from Q^2 units no P_3^b was found, it is clear that when the sodium phosphate glass composition favors the appearance of Q^1 units, the P_3 center will be identified as a center having a slightly lower Fermi contact (~65−70 mT) with respect to the ideal stoichiometric case. This could occur for a ratio $[Na_2O]/[P_2O_5]$ in the range 1−1.5 or in the co-presence of other alkali modifiers, for example, K and Rb.[27,32,33] At variance, with the stoichiometric composition $[Na_2O]/[P_2O_5] = 1$, where the glass features only Q^2 units, only P_3^a configurations can be generated, and P_3 is identified as a paramagnetic center having a Fermi contact of ~74 mT.[27,33]

On the basis of the experimental data available in the paper of Weeks and Bray,[33] no P_3 center can be detected in the irradiated pure P_2O_5 glass. In the light of the present work, the following explanation seems the most probable. As pure P_2O_5 glass consists only of Q^3 units, the occurrence of a nonbridging oxygen vacancy, under irradiation conditions, may result in a P_1 center and never in a P_3 center (neither in P_3^a nor in P_3^b configurations), which is the result of the ionization of an oxygen vacancy at a nonbridging oxygen site of a Q^2 (or Q^1) unit. Once Na is added, Q^2 units are formed, and for Na_2O content of 50%, only Q^2 units are available,[26] so that the generation of P_1 centers becomes unlikely, being substituted with the generation of P_3^a centers. Thus, the latter becomes one of the main[71] intrinsic paramagnetic point defects, related to oxygen vacancies, which can be generated for an alkali content of ~50%.[30,33] For a larger alkali content, an increasing fraction of Q^1 unit will be available for the generation of point defects, in particular of the P_3^b centers (for $1.6Na_2O{:}P_2O_5$ glass, considering a fraction of ~50% of Q^2 and ~50% of Q^1, one could expect to observe global P_3 hfs of $\sim 0.5 \times 74 + 0.5 \times 67 = 70.5$ mT, which could reasonably explain the value given in Table 1 of ref 33 for the hfs of P_3 in $1.6Na_2O{:}P_2O_5$ glass).

In γ-irradiated $NaPO_3$ glasses at 77 K, two metastable centers, called P_α and P_β centers, were observed, which, upon heating above room temperature, are converted to the (stable) P_γ center.[64,65] On the basis of the 3p and 3s wave function hybridization ratio and 3s character, the P_β and P_γ centers were attributed to a three-fold-coordinated P center, whereas P_α was assigned to a four-fold-coordinated center (though, we remark with a 3s character intermediate between those of a three-fold- and a four-fold-coordinated P). Although the study of thermally induced conversions of paramagnetic centers is beyond the scope of the present paper, we remark the following analogies. First, the P_γ center shows hfs of about 75 mT[65] and thus should be regarded as an alias for Week's P_3 center,[33] that is, as due to stable P_3^a configurations. Next, the P_β center shows smaller hfs than P_γ (Figure 2 of ref 64) and thus could be interpreted as due to P_3^b configurations. As for the P_α center, we speculate that it could be interpreted in terms of nonrelaxed P_3^a configuration, which indeed may exhibit a spin density resembling the one of a four-fold-coordinated P center (Figure 4a) and may relax to configurations with larger d (Figure 5a), appearing as stable three-fold-coordinated P_3^a configurations (*i.e.*, P_γ centers). Noteworthily, the results of the EPR measurements before and after annealing[64,65] would also imply that P_3^b could convert to P_3^a configurations.

According to Weeks and Bray,[33] the P_1 and P_3 centers in $xNa_2O{:}P_2O_5$ (x = 0.3, 1.0, 1.3, 1.6) have a similar average $\langle g \rangle \sim 2.01$ (Table 5). These results for $\langle g \rangle$ seem less accurate than for $\langle g \rangle$ of P_1 in pure P_2O_5 glass where $\langle g \rangle \sim 2.005$.[33] The isotropic hyperfine interactions and $\langle g \rangle$ values given in ref 33 were obtained using an approximation to the Breit−Rabi equation[72] and do not provide any insight on the underlying distributions arising due to the different local environments (inhomogeneous broadening) of the unpaired spin. Moreover, EPR investigations in glucose-1-phosphate of a radical ($PO3^{2-}$) analogous to P_1/P_3 centers also suggest, after second-order correction, that the g tensor principal values should be around 2.001 rather than around 2.01.[73] The fact that the g tensor values of the P_1 center are at most ~2.005 in P_2O_5 is also further supported by comparison with P-doped silica (10% P_2O_5 content), where Griscom *et al.*[58,66] provide the following g tensor principal values: $g_\parallel = 2.002$ and $g_\perp = 1.999$ for the P_1 center. Moreover, in the present work, we have calculated average g tensor values: $g_1 \sim 2.0041$, $g_2 \sim 2.0026$, and $g_3 \sim 2.0017$ for the P_1 configuration in our model of P_2O_5, all three well below 2.005. As for the g tensor of P_3 centers, despite the lack of experimental data, besides the Weeks and Bray's paper,[33] we note that Hosono *et al.*[74] report g tensor principal values of $g_\parallel = 2.002$ and $g_\perp = 2.004$ for an analogous center (the so-called HPO_2) in P-doped silica, which are rather close to the g tensor principal values calculated here for the $P_3{}^a$ and $P_3{}^b$ configurations (Table 5).

Pukhkaya *et al.*[29] reported a shift from 74 to 84 mT for A_{iso} with increasing doses (Figure 8 of ref 29) in a meta-phosphate glass featuring a network made of Q^2 units only. This shift suggests that the structure of the P_3 center and of its local environment, under irradiation, could be affected by a disorder increase, which may result from noticeable variations of the interatomic distances, as was evidenced by Raman spectroscopy.[75] In fact, the latter hypothesis is also supported by our findings that P_3^a configurations can feature a larger Fermi contact due to the diminishing of the distance between the threefold coordinated P and a nearby fourth oxygen atom (Figure 5).

We have shown that the P_3 center is analogous to the P_1 center, the structure of both being based on a three-fold P atom. In particular, their spin densities are very similar, so it is likely that the optical absorption bands due to P_3^a and P_3^b will be rather close in energy to the bands due to the P_1 center,[38,39,58] in analogy with what happens to the optical absorption of the E'_α and E'_γ centers in SiO_2.[76] Hence, we can infer that not only the optical absorption of the P_1 centers but also the optical absorption of the P_3 centers can be exploited or diminished in applications such as laser welding by means of phosphate glasses[13] and the production of solid lasers and optical fibers.[77]

5. CONCLUSIONS

In this work, by means of first-principles EPR calculations, we have provided evidence in favor of an interpretation of the P_3 center in terms of ionized nonbridging oxygen vacancies. Furthermore, this work has shown that two kinds of P_3 centers can exist in alkali phosphate glasses such as the $(Na_2O)_x-(P_2O_5)_{(1-x)}$ glasses, that is, the P_3^a and P_3^b centers. In the latter centers, the three-fold-coordinated P atom is bonded to one nonbridging and two bridging oxygen atoms (P_3^a) or to two nonbridging and one bridging oxygen atom (P_3^b).

https://doi.org/10.1021/acs.jpcc.0c11281
J. Phys. Chem. C 2021, 125, 8741−8751

The suggested scenario implies that for an intermediate content of Na_2O, $0 < x < 50\%$, a mixture of P_1 and P_3^a centers should be generated under irradiation, but from an experimental point of view, it may result in a difficulty to resolve both P_1 and P_3 EPR signatures, especially for low concentrations of Na_2O. In fact, in the work of Pukhkaya *et al.*[29] in UP66 glass, which has 67% content of P_2O_5, only P_1 was detected, whereas no clear signature of P_3 has been found. For $x > 50\%$, essentially only P_3^a and P_3^b centers would be generated, whereas P_1 centers would be absent.

Our results indicate a substantial similarity of g tensors in P_1, P_3^a, and P_3^b configurations. The g tensors of P_1, P_3^a, and P_3^b in $NaPO_3$ glass suggest a slightly larger orthorhombicity with respect to P_1 in pure P_2O_5 glass. The orthorhombicity is larger in P_3^b than in P_3^a, suggesting a relation with the number of nonbridging oxygen atoms in the three-fold-coordinated P configurations P_1, P_3^a, and P_3^b.

Finally, our investigation shows the importance of the local environment correlations underlying the distributions of the hyperfine tensors and provides an improved mapping of P centers in phosphate glasses, which may pave the way for fine-controlling/tuning the optical absorption in future technological applications.

■ ASSOCIATED CONTENT

Supporting Information

The Supporting Information is available free of charge at https://pubs.acs.org/doi/10.1021/acs.jpcc.0c11281.

> Spin densities calculated for a P_1 configuration in model RMC1−P_2O_5 and a P_3^a configuration in model RMC2−P_2O_5 in v-P_2O_5; sum of the bond angles O−P−O at a P_3^a center *versus* distance d from the P atom to the fourth next-nearest-neighbor oxygen atom; sum of the bond angles O−P−O *versus* $A_{iso}(^{31}P)$ in P_3^a configurations; Fermi contacts as calculated using the PBE0 hybrid functional and PBE at a relaxed PBE geometry for the selected P_1, P_3^a, and P_3^b configurations in a P-doped α-quartz SiO_2 supercell and in models RMC-SP and CMD-SP of $NaPO_3$ glass; and calculation of $A_{iso}(^{31}P)$ for the radical PH_3^+ (PDF)

■ AUTHOR INFORMATION

Corresponding Author

Luigi Giacomazzi − *Materials Research Laboratory, University of Nova Gorica, Ajdovščina SI-5270, Slovenia;* orcid.org/0000-0003-2499-4276; Email: luigi.giacomazzi@ung.si

Authors

Nikita S. Shcheblanov − *Laboratoire des Solides Irradiés CEA-CNRS, École Polytechnique, Université Paris-Saclay, Palaiseau F-91128, France; NAVIER, (UMR 8205), École des Ponts ParisTech, Univ. Gustave Eiffel, CNRS, UPE, Champs-sur-Marne F-77420, France*

Layla Martin-Samos − *CNR-IOM/Democritos National Simulation Center, Istituto Officina Dei Materiali, Trieste IT-34136, Italy;* orcid.org/0000-0002-1264-0457

Mikhail E. Povarnitsyn − *Moscow Institute of Physics and Technology, Dolgoprudny 141700, Moscow Region, Russia; Joint Institute for High Temperatures, Moscow 125412, Russia*

Shinji Kohara − *Synchrotron X-ray Group, Light/Quantum Beam Field Research Center for Advanced Measurement and Characterization National Institute for Materials Science, Hyogo 679-5198, Japan;* orcid.org/0000-0001-9596-2680

Matjaž Valant − *Materials Research Laboratory, University of Nova Gorica, Ajdovščina SI-5270, Slovenia;* orcid.org/0000-0003-4842-5676

Nicolas Richard − *CEA, DAM, DIF, Arpajon Cedex F-91297, France*

Nadège Ollier − *Laboratoire des Solides Irradiés CEA-CNRS, École Polytechnique, Université Paris-Saclay, Palaiseau F-91128, France*

Complete contact information is available at: https://pubs.acs.org/10.1021/acs.jpcc.0c11281

Notes

The authors declare no competing financial interest.

■ ACKNOWLEDGMENTS

We acknowledge support through the ARRS-CEA Bilateral Project "REPHLES" NC-0008 and financing of the Slovenian Research Agency (ARRS) through the Research Core Funding n. P2-0412. M.E.P. acknowledges support by The Ministry of Science and Higher Education of the Russian Federation (Agreement with Joint Institute for High Temperatures RAS No 075-15-2020−785 dated September 23, 2020). We also acknowledge the MAMMASMIAS consortium and the CNR-IOM DEMOCRITOS Simulation Center for providing high-performance computing resources and support in general. N.S. and L.G. acknowledge Prof. U. Hoppe for the diffraction data, and L.G. acknowledges useful discussions with A. Alessi (LSI/Ecole polytechnique).

■ REFERENCES

(1) *Springer Handbook of Glass*; David Musgraves, J.; Hu, J.; Calvez, L.; Springer International Publishing: Switzerland, 2019.

(2) *Specialty Optical Fibers Handbook* Méndez, A.; Morse, T. F., Eds.; Academic Press: Amsterdam, 2007.

(3) Price, P. B.; Cook, L. M.; Markert, A. Phosphate glasses for identification of heavy ions. *Nature* **1987**, *325*, 137−138.

(4) Swenson, J.; Adams, S. Mixed alkali effect in glasses. *Phys. Rev. Lett.* **2003**, *90*, 155507.

(5) Nakata, S.; Togashi, T.; Honma, T.; Komatsu, T. Cathode properties of sodium iron phosphate glass for sodium ion batteries. *J. Non-Cryst. Solids* **2016**, *450*, 109−115.

(6) Onodera, Y.; Kohara, S.; Masai, H.; Koreeda, A.; Okamura, S.; Ohkubo, T. Formation of metallic cation-oxygen network for anomalous thermal expansion coefficients in binary phosphate glass. *Nat. Commun.* **2017**, *8*, 15449.

(7) Inaba, S.; Hosono, H.; Ito, S. Entropic shrinkage of an oxide glass. *Nat. Mater.* **2015**, *14*, 312−317.

(8) Aoyagi, T.; Kohara, S.; Naito, T.; Onodera, Y.; Kodama, M.; Onodera, T.; Takamatsu, D.; Tahara, S.; Sakata, O.; Miyake, T.; et al. Controlling oxygen coordination and valence of network forming cations. *Sci. Rep.* **2020**, *10*, 7178.

(9) Di Sieno, L.; Boetti, N. G.; Dalla Mora, A.; Pugliese, D.; Farina, A.; Konugolu Venkata Sekar, S.; Ceci-Ginistrelli, E.; Janner, D.; Pifferi, A.; Milanese, D. Towards the use of bioresorbable fibers in time-domain diffuse optics. *J. Biophot.* **2017**, *11*, No. e201600275.

(10) Franczyk, M.; Stępień, R.; Piechal, B.; Pysz, D.; Stawicki, K.; Siwicki, B.; Buczyński, R. High efficiency Yb^{3+}-doped phosphate single-mode fibre laser. *Laser Phys. Lett.* **2017**, *14*, 105102.

(11) Dragic, P. D.; Cavillon, M.; Ballato, J. Materials for optical fiber lasers: a review. *Rev. Phys. Appl.* **2018**, *5*, 041301.

(12) Galleani, G.; Doerenkamp, C.; Santagneli, S.; Magon, C. J.; de Camargo, A. S. S.; Eckert, H. Compositional optimization of emission properties for rare-earth doped fluoride phosphate glasses: Structural investigations via NMR, EPR, and optical spectroscopies. *J. Phys. Chem. C* **2019**, *123*, 31219−31231.
(13) Dabich, L. C.; et al. Sealed devices comprising transparent laser weld regions. U.S. Patent US20190074476 A1 (Mar. 7, 2019) https://patents.google.com/patent/US20190074476A1/en. (accessed February 2021).
(14) Miyamoto, Y.; Takei, Y.; Nanto, H.; Kurobori, T.; Konnai, A.; Yanagida, T.; Yoshikawa, A.; Shimotsuma, Y.; Sakakura, M.; Miura, K.; et al. Radiophotoluminescence from silver-doped phosphate glass. *Radiat. Meas.* **2011**, *46*, 1480−1483.
(15) Ivascu, C.; Cozar, I. B.; Daraban, L.; Damian, G. Spectroscopic investigation of P_2O_5-CdO-Li_2O glass system. *J. Non-Cryst. Solids* **2013**, *359*, 60−64.
(16) Van Wazer, J. R. Structure and properties of the condensed phosphates. II. A theory of the molecular structure of sodium phosphate glasses. *J. Am. Chem. Soc.* **1950**, *72*, 644−647.
(17) Brady, G. W. Structure of sodium metaphosphate glass. *J. Chem. Phys.* **1958**, *28*, 48−50.
(18) Milberg, M. E.; Daly, M. C. Structure of oriented sodium metaphosphate glass fibers. *J. Chem. Phys.* **1963**, *39*, 2966−2973.
(19) Inaba, S.; Benino, Y.; Kohara, S.; Hosono, H.; Ito, S. Anisotropic structure of alkali metaphosphate glasses. *J. Am. Ceram. Soc.* **2020**, *103*, 3631−3641.
(20) Loong, C.-K.; Suzuya, K.; Price, D. L.; Sales, B. C.; Boatner, L. A. Structure and dynamics of phosphate glasses: From ultra- to orthophosphate composition. *Phys. B Condens. Matter* **1997**, *241*−*243*, 890−896.
(21) Hudgens, J. J.; Brow, R. K.; Tallant, D. R.; Martin, S. W. Raman spectroscopy study of the structure of lithium and sodium ultraphosphate glasses. *J. Non-Cryst. Solids* **1998**, *223*, 21−31.
(22) Mandal, A.; Kiran Gogi, V.; Mohanty, C.; Chbeir, R.; Boolchand, P. Emerging role of local and extended range molecular structures on functionalities of topological phases of $(Na_2O)_x(P_2O_5)_{100-x}$ glasses using Raman scattering and modulated DSC. *Int. J. Appl. Glass Sci.* **2021**, *12*, 89−110.
(23) Uchino, T.; Ogata, Y. Ab-initio molecular orbital calculations on the electronic structure of phosphate glasses. Sodium phosphate glasses. *J. Non-Cryst. Solids* **1995**, *181*, 175−188.
(24) Uchino, T.; Yoko, T. Structure and vibrational properties of alkali phosphate glasses from ab initio molecular orbital calculations. *J. Non-Cryst. Solids* **2000**, *263*−*264*, 180−188.
(25) Flambard, A.; Montagne, L.; Delevoye, L.; Palavit, G.; Amoureux, J.-P.; Videau, J.-J. Solid-state NMR study of mixed network sodium-niobium phosphate glasses. *J. Non-Cryst. Solids* **2004**, *345*−*346*, 75−79.
(26) Hermansen, C.; Mauro, J. C.; Yue, Y. A model for phosphate glass topology considering the modifying ion sub-network. *J. Chem. Phys.* **2014**, *140*, 154501.
(27) Mohanty, C.; Mandal, A.; Kiran Gogi, V.; Chen, P.; Novita, D.; Chbeir, R.; Bauchy, M.; Micoulaut, M.; Boolchand, P. Linking melt dynamics with topological phases and molecular structure of sodium phosphate glasses from calorimetry, Raman scattering, and infrared reflectance. *Front. Mater. Sci.* **2019**, *6*, 69.
(28) Shcheblanov, N. S.; Giacomazzi, L.; Povarnitsyn, M. E.; Kohara, S.; Martin-Samos, L.; Mountjoy, G.; Newport, R. J.; Haworth, R. C.; Richard, N.; Ollier, N. Vibrational and structural properties of P_2O_5 glass: advances from a combined modeling approach. *Phys. Rev. B* **2019**, *100*, 134309.
(29) Pukhkaya, V.; Trompier, F.; Ollier, N. New insights on P-related paramagnetic point defects in irradiated phosphate glasses: Impact of glass network type and irradiation dose. *J. Appl. Phys.* **2014**, *116*, 123517.
(30) Watanabe, Y.; Kanazawa, T.; Kawazoe, H. Structure of radiation-induced ESR centers in nitrogen-containing phosphate glasses. *J. Non-Cryst. Solids* **1985**, *71*, 279−286.
(31) Nakai, Y. Electron paramagnetic resonance study of γ-ray irradiated phosphate glasses. *Bull. Chem. Soc. Jpn.* **1965**, *38*, 1308−1313.
(32) Hasegawa, A.; Miura, M. The electron spin resonance of γ-irradiated sodium polyphosphate. II. Effects of the degree of polymerization and the kind of cation. *Bull. Chem. Soc. Jpn.* **1967**, *40*, 2553−2558.
(33) Weeks, R. A.; Bray, P. J. Electron spin resonance spectra of gamma-ray-irradiated phosphate glasses and compounds: Oxygen vacancies. *J. Chem. Phys.* **1968**, *48*, 5−13.
(34) Linganna, K.; Ju, S.; Basavapoornima, C.; Jayasankar, C. K.; Venkatramu, V.; Kim, C. J.; Han, W.-T. Optical absorption and EPR studies on gamma-ray irradiated RE^{3+}-doped fluorophosphate glasses. *J. Inorg. Organomet. Polym. Mater.* **2018**, *28*, 594−602.
(35) Möncke, D.; Reibstein, S.; Schumacher, D.; Wondraczek, L. Irradiation-induced defects in ionic sulfophosphate glasses. *J. Non-Cryst. Solids* **2014**, *383*, 33−37.
(36) Ebeling, P.; Ehrt, D.; Friedrich, M. Study of radiation-induced defects in fluoride-phosphate glasses by means of optical absorption and EPR spectroscopy. *Glass Sci. Technol.* **2000**, *73*, 156−162.
(37) Bocharova, T. V.; Vlasova, A. N.; Karapetyan, G. O.; Maslennikova, O. N.; Sirotkin, S. A.; Tagil'tseva, N. O. Influence of Small Additives of Rare-Earth Elements on the Structure of Fluorophosphate Glasses. *Glass Phys. Chem.* **2010**, *36*, 286−293.
(38) Masai, H.; Okada, G.; Kawaguchi, N.; Yanagida, T. Relationship between defect formation by X-ray irradiation and thermally stimulated luminescence of binary zinc phosphate glasses. *Opt. Mater. Express* **2019**, *9*, 2037.
(39) Ebeling, P.; Ehrt, D.; Friedrich, M. X-ray induced effects in phosphate glasses. *Opt. Mater.* **2002**, *20*, 101−111.
(40) Ebeling, P.; Ehrt, D.; Friedrich, M. Influence of modifier cations on the radiation-induced effects of metaphosphate glasses. *Glass Sci. Technol.* **2003**, *76*, 56−61.
(41) Also[39,40] report of an electron trapped center at a four-fold P (i.e. aP_2 center) with $A_{iso} \sim 126$ mT and $\langle g \rangle \sim 2.142$ much larger than 2.01 to 2.04 provided by Weeks and Bray.[33] Note that $\langle g \rangle$ is obtained in[39,40] as middle value between g tensor values of both lines of a doublet, i.e. $\langle g \rangle = (g_l + g_r)/2$.
(42) Giannozzi, P.; Baroni, S.; Bonini, N.; Calandra, M.; Car, R.; Cavazzoni, C.; Ceresoli, D.; Chiarotti, G. L.; Cococcioni, M.; Dabo, I.; et al. A modular and open-source software project for quantum simulations of materials. *J. Phys. Condens. Matter* **2009**, *21*, 395502.
(43) Giannozzi, P.; Andreussi, O.; Brumme, T.; Bunau, O.; Buongiorno Nardelli, M.; Calandra, M.; Car, R.; Cavazzoni, C.; Ceresoli, D.; Cococcioni, M.; et al. Advanced capabilities for materials modeling with Quantum ESPRESSO. *J. Phys. Condens. Matter* **2017**, *29*, 465901.
(44) Perdew, J. P.; Burke, K.; Ernzerhof, M. Generalized gradient approximation made simple. *Phys. Rev. Lett.* **1996**, *77*, 3865−3868.
(45) Giacomazzi, L.; Martin-Samos, L.; Alessi, A.; Valant, M.; Boukenter, A.; Ouerdane, Y.; Girard, S.; Richard, N.; De Gironcoli, S. v-P_2O_5 microclustering in P-doped silica studied by a first-principles Raman investigation. *Sci. Rep.* **2019**, *9*, 7126.
(46) Gafurov, M.; Biktagirov, T.; Mamin, G.; Orlinskii, S. A DFT, X- and W-band EPR and ENDOR study of nitrogen-centered species in (nano)hydroxyapatite. *Appl. Magn. Reson.* **2014**, *45*, 1189−1203.
(47) The set of adopted (scalar relativistic) pseudopotentials employed in this work: P.pbe-tm-gipaw.UPF, O.pbe-tm-gipaw.UPF, Si.pbe-tm-gipaw.UPF and Na.pbe-tm-gipaw-dc.UPF is available at: https://sites.google.com/site/dceresoli/pseudopotentials.
(48) Kohara, S.; Akola, J.; Morita, H.; Suzuya, K.; Weber, J. K. R.; Wilding, M. C.; Benmore, C. J. Relationship between topological order and glass forming ability in densely packed enstatite and forsterite composition glasses. *Proc. Natl. Acad. Sci. U.S.A.* **2011**, *108*, 14780.
(49) Kohara, S.; Salmon, P. S. Recent advances in identifying the structure of liquid and glassy oxide and chalcogenide materials under extreme conditions: A joint approach using diffraction and atomistic simulation. *Adv. Phys.: X* **2016**, *1*, 640−660.

https://doi.org/10.1021/acs.jpcc.0c11281
J. Phys. Chem. C 2021, 125, 8741−8751

(50) Gereben, O.; Jóvári, P.; Temleitner, L.; Pusztai, L. A new version of the RMC++ Reverse Monte Carlo programme, aimed at investigating the structure of covalent glasses. *J. Optoelectron. Adv. Mater.* **2007**, *9*, 3021−3027.
(51) Hoppe, U.; Delevoye, L.; Montagne, L.; Zimmermann, M. V.; Hannon, A. C. Structure of Nb_2O_5-$NaPO_3$ glasses by X-ray and neutron diffraction. *Phys. Chem. Chem. Phys.* **2013**, *15*, 8520−8528.
(52) Al Hasni, B.; Martin, R. A.; Storey, C.; Mountjoy, G.; Pickup, D.M.; Newport, R.J. Molecular dynamics modelling of sodium and calcium metaphosphate glasses for biomaterial applications. *Phys. Chem. Glasses: Eur. J. Glass Sci. Technol., Part B* **2016**, *57*, 245−253.
(53) Plimpton, S. Fast parallel algorithms for short-range molecular dynamics. *J. Comput. Phys.* **1995**, *117*, 1−19.
(54) The hyperfine spin-Hamiltonian $H_{hf} = \mathbf{S}\cdot\mathbf{A}\cdot\mathbf{I}$ arises from the coupling between the electron spin **S** and the nuclear spin **I** through the hyperfine tensor **A** which can be decomposed into an isotropic part A_{iso} (i.e. the Fermi contact) and a traceless anisotropic tensor **B**. The latter results from the dipolar interaction and in a one-electron system can be written as: $B_{ij} = \frac{\mu}{4\pi} g_N \beta_N g_e \beta_e \int (3x_i x_j/r^5 - \delta_{ij}/r^3)|\psi(\mathbf{r})|^2 \, dV$ where μ is the permeability of free space, g_N and g_e are the nuclear and the electronic *g*-factors, β_N and β_e are the nuclear and Bohr magnetons. In its principal axes the tensor *B* can be described using its principal values B_1, B_2, B_3.
(55) Pickard, C. J.; Mauri, F. First-principles theory of the EPR *g* tensor in solids: Defects in quartz. *Phys. Rev. Lett.* **2002**, *88*, 086403.
(56) Giacomazzi, L.; Martin-Samos, L.; Boukenter, A.; Ouerdane, Y.; Girard, S.; Richard, N. EPR parameters of *E′* centers in *v*-SiO_2 from first-principles calculations. *Phys. Rev. B: Condens. Matter Mater. Phys.* **2014**, *90*, 014108.
(57) Pacchioni, G.; Erbetta, D.; Ricci, D.; Fanciulli, M. Electronic structure of defect centers P_1, P_2, and P_4 in P-doped SiO_2. *J. Phys. Chem. B* **2001**, *105*, 6097−6102.
(58) Griscom, D. L.; Friebele, E. J.; Long, K. J.; Fleming, J. W. Fundamental defect centers in glass: Electron spin resonance and optical absorption studies of irradiated phosphorus doped silica glass and optical fibers. *J. Appl. Phys.* **1983**, *54*, 3743−3762.
(59) Giacomazzi, L.; Martin-Samos, L.; Alessi, A.; Valant, M.; Gunturu, K. C.; Boukenter, A.; Ouerdane, Y.; Girard, S.; Richard, N. Optical absorption spectra of P defects in vitreous silica. *Opt. Mater. Express* **2018**, *8*, 385.
(60) Speghini, A.; Sourial, E.; Peres, T.; Pinna, G.; Bettinelli, M.; Capobianco, J. A. Structural investigation of $NaPO_3$ glass using molecular dynamics simulation. *Phys. Chem. Chem. Phys.* **1999**, *1*, 173−177.
(61) Mulevanon, S. V. Structure of short-range order in phosphorus oxide doped silicate glasses. *Glass Ceram.* **2009**, *66*, 375−377.
(62) Fan, G.; Diao, J.; Jiang, L.; Zhang, Z.; Xie, B. Molecular dynamics analysis of the microstructure of the CaO-P_2O_5-SiO_2 slag system with varying P_2O_5/SiO_2 ratios. *Mater. Trans.* **2015**, *56*, 655−660.
(63) Tilocca, A. Structure and dynamics of bioactive phosphosilicate glasses and melts from ab initio molecular dynamics simulations. *Phys. Rev. B: Condens. Matter Mater. Phys.* **2007**, *76*, 224202.
(64) Hosono, H.; Abe, Y.; Kawazoe, H. ESR study of radiation induced paramagnetic defect centers localized on a phosphorus in binary phosphate glasses. *J. Non-Cryst. Solids* **1985**, *71*, 261−267.
(65) Hosono, H.; Abe, Y. Paramagnetic centers localized on a phosphorus ion in gamma-irradiated metaphosphate glasses. *J. Ceram. Soc. Jpn.* **1985**, *93*, 217−224.
(66) Stesmans, A.; Clémer, K.; Afanas'ev, V. V. P-associated defects in the high-*k* insulators HfO_2 and ZrO_2 revealed by electron spin resonance. *Phys. Rev. B: Condens. Matter Mater. Phys.* **2008**, *77*, 125341.
(67) The calculated *g* tensor for the P_1 center in P-doped silica are the average of the values found for *p4x* configurations,[56] representative for the *E′*−Si, which were transformed into P_1 configurations after substitution of three-fold Si with three-fold P.
(68) The coordination (with oxygens) of the P atom is defined by a cutoff distance of 2.2 Å. With such a cutoff, about twenty $P_3{}^a$ configurations in Model CMD-SP are identified.
(69) Giacomazzi, L.; Martin-Samos, L.; Richard, N. Paramagnetic centers in amorphous GeO_2. *Microelectron. Eng.* **2015**, *147*, 130−133.
(70) Giacomazzi, L.; Martin-Samos, L.; Boukenter, A.; Ouerdane, Y.; Girard, S.; Richard, N. Ge(2), Ge(1) and Ge-*E′* centers in irradiated Ge-doped silica: A first-principles EPR study. *Opt. Mater. Express* **2015**, *5*, 1054.
(71) In general, the glass matrix may contain impurities or small quantities of dopants such as RE ions so that other irradiation induced paramagnetic centers are generated together with P_3, P_2, P_1 and POHC centers.
(72) Breit, G.; Rabi, I. I. Measurement of nuclear spin. *Phys. Rev.* **1931**, *38*, 2082−2083.
(73) Bungum, B.; Hole, E. O.; Sagstuen, E.; Lindgren, M. Electron paramagnetic resonance of X-irradiated sodium and potassium salts of glucose-1-phosphate. Identification of radicals at room temperature. *Radiat. Res.* **1994**, *139*, 194−202.
(74) Hosono, H.; Kajihara, K.; Hirano, M.; Oto, M. Photochemistry in phosphorus-doped silica glass by ArF excimer laser irradiation: Crucial effect of H_2 loading. *J. Appl. Phys.* **2002**, *91*, 4121−4124.
(75) Mahfoudhi, M. Eu^{3+} ion environment modification by Electron and femtosecond laser irradiation in metaphosphate and polyphosphate glasses. Ph.D. Thesis, Université Paris-Saclay, Paris, France, 2019 at p. 114.
(76) Buscarino, G.; Boscaino, R.; Agnello, S.; Gelardi, F. M. Optical absorption and electron paramagnetic resonance of the *E′* center in amorphous silicon dioxide. *Phys. Rev. B: Condens. Matter Mater. Phys.* **2008**, *77*, 155214.
(77) Regnier, E.; Flammer, I.; Girard, S.; Gooijer, F.; Achten, F.; Kuyt, G. Low-dose radiation-induced attenuation at infrared wavelengths for P-doped, Ge-doped and pure silica-core optical fibres. *IEEE Trans. Nucl. Sci.* **2007**, *54*, 1115−1119.

https://doi.org/10.1021/acs.jpcc.0c11281
J. Phys. Chem. C 2021, 125, 8741−8751